# Phase Behavior of Mixtures of Low Molar Mass Nematic Liquid Crystal and in Situ Photo-Cross-Linked Polymer Network

**Domasius Nwabunma and Thein Kyu***

*Institute of Polymer Engineering, The University of Akron, Akron, Ohio 44325*

*Received October 2, 1998; Revised Manuscript Received December 15, 1998*

ABSTRACT: Phase equilibria and mesophase ordering behavior of mixtures of low molar mass nematic liquid crystal (LC) and photo-cross-linked polymeric network have been investigated theoretically and experimentally. The nematic LC used was a single component, viz., 4-*n*-heptyl-4′-cyanobiphenyl (K21). The polymer network was formed by photo-cross-linking multifunctional thiolene-based optical adhesive (NOA65). On the basis of a simple addition of the free energy densities of isotropic mixing and nematic ordering along with the elastic free energy density of the network, phase diagrams have been established by solving the total free energy equation self-consistently. The effects of average repeat units between cross-linked points, network functionality, and concentration dependence of network models on the phase diagrams of LC/polymer network were examined. The calculated phase diagrams displayed isotropic network + nematic solvent (I + N), isotropic network + isotropic solvent (I + I), and isotropic swollen network (I) coexistence regions. Decreasing the segment length between cross-linked points or increasing the network functionality leads to a tight (dense) network that accommodates less LC solvent molecules. However, the segment length between the cross-links exerts a greater influence on the phase diagrams than the network functionality. A comparison has been made between the phase diagrams of LC/linear polymer and LC/cross-linked polymer systems. Of particular interest is that the coexistence curve of the LC/cross-linked polymer shows no critical point. Instead, it exhibits an upward turn in curvature as the LC volume fraction approaches unity. This behavior seems to be dominated by the contribution arising from the elastic free energy of the polymer network, which is entropic in origin. Light scattering and optical microscopic experiments have been carried out to test theoretical predictions. A good agreement between theory and experiment attests to the predictive capability of the theory.

## Introduction

Liquid crystal (LC)/polymer composites have been the focus of immense theoretical and experimental investigations because of their potential in various electrooptical display and control applications.[1−6] These studies include synthesis of new materials, phase behavior, morphological characterization, polymerization kinetics, phase separation dynamics, electrooptical characterization, and optimization of device performance. In general, these composite films have been fabricated via microencapsulation or via phase separation induced by thermal quenching or polymerization through thermal initiation or photoinitiation based on ultraviolet (UV) radiation.

Most works hitherto reported on phase behavior of LC/polymer composites are those formed via thermal quench-induced phase separation and/or through solvent removal that generally involve linear polymers as a matrix.[7−11] Polymerization-induced phase separation (PIPS) is a nonlinear dynamic process that requires not only a knowledge of reaction kinetics but also an understanding of thermodynamic phase equilibria of the LC/monomer mixture before cure. Hence, much attention has been devoted to the establishment of the phase diagrams of the starting LC/monomer mixtures[12−15] prior to the studies on dynamics of PIPS.

In principle, the thermodynamic state of the starting LC/monomer mixtures has a profound influence on the emergence of domain morphology driven by PIPS. The emerging morphology depends strongly on the polymerization temperature and composition; that is to say, the domain morphology is drastically different whether the reaction is initiated in the isotropic region or in the two-phase region.[15] Early studies on the effect of polymerization on nematic LC/polymer phase diagrams have assumed linear polymerization for simplicity.[16] However, it is well documented that polymerization of multifunctional monomers in the presence of LC not only leads to linear chain propagation but also results in a three-dimensional cross-linked network. The elastic free energy of the polymer network, which is entropic in origin, should therefore contribute to thermodynamics of LC/cross-linked polymer system. Such additional effects ought to be addressed in the calculation of the LC/polymer network phase diagrams.

While recognizing the role of network elasticity on the phase diagram of LC/polymer networks, it has been largely ignored in the literature until recently.[17−19] Bauer et al.[20,21] examined the role of elastic free energy of a network on the phase diagram of binary polymer/network blends. Boots et al.[17] extended the elastic free energy contribution of the network on conversion phase diagrams of the LC/monomer system subjected to photopolymerization. However, for simplicity the liquid crystal ordering was ignored in their calculation. Recently, the aforementioned drawback (i.e., the exclusion of the free energy of liquid crystal ordering) has been accounted for in a recent work of Benmouna et al.[18] These authors extended the early theoretical work of Shen and Kyu[9] for the establishment of phase diagrams of mixtures of nematic/linear polymer to the nematic/polymer network by taking into consideration the free energy of mesophase ordering in conjunction with those of isotropic mixing and network elasticity proposed originally by Bauer et al.[20,21] Further, following the approach of Kyu and Chiu,[10] they extended the theory

* To whom correspondence should be addressed.

10.1021/ma981556y CCC: $18.00 
Published on Web 01/20/1999

of smectic/linear polymer system to the smectic/polymer network mixture.[19]

In this work, we first solve self-consistently the theoretical phase diagrams of a nematic/flexible monomer mixture on the basis of the free energies of mixing and nematic ordering. It is subsequently extended to the mixture of nematic LC/in situ photo-cross-linked flexible network by taking into consideration the additional free energy contribution arising from the network elasticity. The effects of segment length between cross-linked points, network functionality, and concentration dependence of network models on the phase diagrams have been examined. An experimental phase diagram of the mixture of a single-component nematic LC (4-*n*-heptyl-4′-cyanobiphenyl (designated K21)) and photo-cross-linked multifunctional thiolene-based optical adhesive (designated NOA65) has been established using optical microscopy and light scattering. Finally, the coexistence regions are identified experimentally to test the predictive capability of the theory.

## Theoretical Scheme

Let us first consider the photo-cross-linking of flexible chains in the presence of the low molar mass nematic LC. It may be assumed that all monomers are consumed during the photo-cross-linking reaction leading to a three-dimensional network, although such a situation may be difficult to realize in practice. Furthermore, the polymer network is assumed to be isotropic and the chains obey Gaussian statistics. This permits us to use the elastic free energy for an isotropic flexible chain network. If the network were nematic in character, then an additional elastic free energy arising from the nematic ordering within the network should be considered. This scenario has been addressed by Warner and Wang[22,23] and is therefore not examined here.

In the theoretical description of phase equilibria of a mixture of nematic LC and cross-linked polymer, a convenient starting point is to consider the total free energy density of the system. The total free energy density, $g$, of the binary system may be expressed as a simple summation of free energy density of isotropic mixing, $g^{\mathrm{i}}$, free energy density of nematic ordering, $g^{\mathrm{n}}$, and free energy density due to network elasticity, $g^{\mathrm{e}}$, as follows:

$$g = g^{\mathrm{i}} + g^{\mathrm{n}} + g^{\mathrm{e}} \tag{1}$$

The free energy density of isotropic mixing, $g^{\mathrm{i}}$, is assumed to be of the Flory−Huggins form.[24,25] However, since we have a network rather than discrete solute molecules, there is no combinatorial entropy of mixing term, $(\phi_{\mathrm{P}} \ln \phi_{\mathrm{P}})/r_{\mathrm{P}}$, for the polymer network;[23,26−28] i.e., it is as if the network is of infinite molecular weight ($r_{\mathrm{P}} = \infty$). Thus, $g^{\mathrm{i}}$ may be written as

$$g^{\mathrm{i}} = \frac{\Delta G^{\mathrm{i}}}{n k_{\mathrm{B}} T} = \frac{\phi_{\mathrm{L}} \ln \phi_{\mathrm{L}}}{r_{\mathrm{L}}} + \chi \phi_{\mathrm{L}} \phi_{\mathrm{P}} \tag{2}$$

where $\Delta G^{\mathrm{i}}$ is the free energy of isotropic mixing, $k_{\mathrm{B}}$ the Boltzmann constant, and $T$ the absolute temperature. Subscripts L and P refer to nematic LC and polymer network, respectively. Thus, $\phi_{\mathrm{L}}$ and $\phi_{\mathrm{P}}$ are their respective volume fractions, whereas $n$ is the total number of molecules given by

$$n = n_{\mathrm{L}} r_{\mathrm{L}} + n_{\mathrm{P}} \tag{3}$$

In eq 3, the polymer network is considered as one giant molecule composed of $n_{\mathrm{p}}$ monomers, while $n_{\mathrm{L}}$ is the number of nematic LC molecules occupying $r_{\mathrm{L}}$ sites. The following relationships are assumed to hold:

$$\phi_{\mathrm{L}} = \frac{n_{\mathrm{L}} r_{\mathrm{L}}}{n}; \quad \phi_{\mathrm{P}} = \frac{n_{\mathrm{P}}}{n} = 1 - \phi_{\mathrm{L}} \tag{4}$$

The Flory−Huggins isotropic mixing interaction parameter, $\chi$, is as usual taken to be an inverse function of temperature of the form

$$\chi = A + B/T \tag{5}$$

where $A$ and $B$ are constants. In this work, we ignored any dependence of $\chi$ on concentration or cross-linked density. The parameter $A$ is used to account for the broadness of the coexistence curve (UCST or LCST), while parameter $B$ can be obtained from the critical interaction parameter, $\chi_{\mathrm{c}}$, and temperature, $T_{\mathrm{c}}$, as $B = (\chi_{\mathrm{c}} - A)/T_{\mathrm{c}}$. In this study, we used the temperature dependence of $\chi$ of the LC/monomer system[15] since our network is made in situ. In their calculations, Benmouna et al.[18,19] used the temperature dependence of $\chi$ of the LC/linear polymer, while Boots et al.[17] and Warner and Wang[22,23] assumed that $\chi$ is a constant independent of temperature. As is well-known, the relationship of $\chi$ vs $T$ used in the calculation could affect the phase diagrams.

The nematic ordering free energy density, $g^{\mathrm{n}}$, is given by the Maier−Saupe theory.[29] The expression for $g^{\mathrm{n}}$ after the incorporation of the nematic LC volume fraction and minimizing for a stable nematic phase is given by[9]

$$g^{\mathrm{n}} = \frac{\Delta G^{\mathrm{n}}}{n k_{\mathrm{B}} T} = \frac{1}{r_{\mathrm{L}}}[-\phi_{\mathrm{L}} \ln z + {}^1/_2 \nu \phi_{\mathrm{L}}{}^2 s^2] \tag{6}$$

where $\Delta G^{\mathrm{n}}$ is the free energy of nematic ordering. The normalized partition function, $z$, and nematic order parameter, $s$, are respectively defined by the following integrals:[9]

$$z = \int_0^1 \exp({}^3/_2 m x^2 - {}^1/_2 m)\, \mathrm{d}x \tag{7}$$

$$s = {}^3/_2 \frac{\int_0^1 x^2 \exp({}^3/_2 m x^2 - {}^1/_2 m)\, \mathrm{d}x}{\int_0^1 \exp({}^3/_2 m x^2 - {}^1/_2 m)\, \mathrm{d}x} - {}^1/_2 \tag{8}$$

where $x = \cos\theta$ and $\theta$ is the angle between the LC directors and the reference $z$ axis. The quantity $m$ is a mean field parameter characterizing the strength of the orientational potential field of the LC directors. Both $s$ and $m$ are further related to LC volume fraction, $\phi_{\mathrm{L}}$, through the following equation:

$$m = \nu \phi_{\mathrm{L}} s \tag{9}$$

where $\nu$ is the Maier−Saupe interaction parameter, which is related to the nematic−isotropic transition temperature, $T_{\mathrm{NI}}$, of the nematic LC via inverse dependence on temperature as follows:

$$\nu = 4.541(T_{\mathrm{NI}}/T) \tag{10}$$

The elastic free energy density, $g^{\mathrm{e}}$, for an isotropic flexible perfect polymeric network with ideal Gaussian

chains is given by[26−28]

$$g^{e} = \frac{\Delta G^{e}}{nk_{B}T} = \left(\frac{3\alpha_{e}}{2r_{c}}\right)\Phi_{0}^{2/3}(\phi_{P}^{1/3} - \phi_{P}) + \left(\frac{\beta_{e}}{r_{c}}\right)\phi_{P} \ln \phi_{P} \tag{11}$$

where $\Delta G^{e}$ is the elastic free energy and $r_c$ is the segment length between cross-links (or chemical junction points). The parameter $\Phi_0$ represents the volume fraction of the network in the reference (unswollen) state, and $\Phi_0 = 1$ if the chains were cross-linked in the bulk. In the present case, the polymeric network is formed in the presence of LC and/or unreacted monomer; thus, it may be regarded as a pseudo-two-phase system. Following the procedure of Boots et al.[17] and Bauer and Briber,[20] we take $\Phi_0 = \phi_P$ assuming that networks are not swollen during photo-cross-linking. In contrast, Benmouna et al.[18,19] used a constant value of $\Phi_0 = {}^1/_2$ and pointed out that the choice of $\Phi_0$ affected significantly the free energy expression and the resulting phase diagram. As we shall see, the choice of the $\Phi_0$ value makes an appreciable difference between our work and that reported earlier by Benmouna et al.[18,19]

Network parameters, $\alpha_e$ and $\beta_e$, have been described in various forms of theoretical models. According to the affine network model of Flory,[30] these parameters are expressed as

$$\alpha_{e} = 1; \quad \beta_{e} = 2/f \tag{12}$$

where $f$ is the network functionality ($3 \le f < \infty$). The phantom network model ($f = \infty$) of James and Guth[31] suggested different values as follows:

$$\alpha_{e} = 1; \quad \beta_{e} = 0 \tag{13}$$

Recently, Petrovic et al.[32] proposed a linear dependence of $\alpha_e$ and $\beta_e$ on volume fraction of the polymer network of the form

$$\alpha_{e} = 1 - \frac{2}{f}(1 - \phi_{P}); \quad \beta_{e} = \frac{2\phi_{P}}{f} \tag{14}$$

It should be noted in eq 14 that the limit $\phi_P \to 1$ corresponds to the Flory affine network model, whereas the limit $\phi_P \to 0$ corresponds to the James and Guth phantom model. Since the three network models are obviously different, it is of interest to investigate their effects on the phase behavior of LC/polymer network mixture.

**Establishment of Theoretical Phase Diagrams.** Equilibrium between two coexisting phases is normally determined by the equality of chemical potential of each component in the two phases. For the nematic LC/cross-linked polymer system, we have a phase of swollen network or isotropic gel (phase I) in equilibrium with a phase of the pure LC solvent (phase II). Note that cross-linked network can no longer be dissolved in the anisotropic solvent. The LC solvent, however, can be dissolved in the network via swelling. The swelling of the network by the LC solvent can occur either in the nematic phase ($T < T_{NI}$ and $\phi_L > \phi_{L,c}$) or in the isotropic phase ($T > T_{NI}$, any $\phi_L$). The quantity $\phi_{L,c} = T/T_{NI}$ is the critical LC volume fraction below which nematic ordering is prohibited. The chemical potentials should be balanced in equilibrium and thus may be described as[26−28]

$$\left(\frac{\Delta\mu_{L}}{k_{B}T}\right)^{I} = \left(\frac{\Delta\mu_{L}}{k_{B}T}\right)^{II} \tag{15}$$

In phase I, the condition below holds:

$$\phi_{L}^{I} + \phi_{P}^{I} = 1 \tag{16}$$

Similarly, the following conditions hold in phase II:

$$\phi_{L}^{II} = 1; \quad \phi_{P}^{II} = 0 \tag{17}$$

$\phi_P^{II} = 0$ implies that the polymer network cannot be dissolved in the LC solvent; that is, there is no network in phase II. The chemical potential of nematic solvent, $\Delta\mu_L/k_BT$ may be expressed as

$$\frac{\Delta\mu_{L}}{k_{B}T} = \frac{\Delta\mu_{L}^{i}}{k_{B}T} + \frac{\Delta\mu_{L}^{n}}{k_{B}T} + \frac{\Delta\mu_{L}^{e}}{k_{B}T} \tag{18}$$

The chemical potential of isotropic mixing of the LC solvent, $\Delta\mu^i/k_BT$, is represented by the following equation[33]

$$\frac{\Delta\mu_{L}^{i}}{k_{B}T} = \frac{\partial(\Delta G^{i}/k_{B}T)}{\partial n_{L}} = \ln \phi_{L} + \phi_{P} + \chi\phi_{P}^{2} \tag{19}$$

The chemical potential for nematic ordering of the LC solvent, $\Delta\mu^n/k_BT$, may be given as[9]

$$\frac{\Delta\mu_{L}^{n}}{k_{B}T} = \frac{\partial(\Delta G^{n}/k_{B}T)}{\partial n_{L}} = -\ln z + {}^1/_2\nu\phi_{L}^{2}s^{2} \tag{20}$$

The elastic chemical potential for the solvent, $\Delta\mu^e/k_BT$, may be expressed in two different forms depending on whether $\alpha_e$ and $\beta_e$ are functions of $\phi_P$. If $\alpha_e$ and $\beta_e$ are independent of $\phi_P$ as proposed in the model of Flory[30] or that of James and Guth,[31] the elastic chemical potential for the solvent is given by[17]

$$\frac{\Delta\mu_{L}^{e}}{k_{B}T} = \frac{\partial(\Delta G^{e}/k_{B}T)}{\partial n_{L}} = \frac{1}{r_{c}}[\alpha_{e}\Phi_{0}^{2/3}\phi_{p}^{-2/3} - \beta_{e}]\phi_{p} \tag{21}$$

On the other hand, if one adopts the Petrovic et al.[30] model, in which $\alpha_e$ and $\beta_e$ vary with $\phi_P$, then the elastic chemical potential of the solvent is given by[17]

$$\frac{\Delta\mu_{L}^{e}}{k_{B}T} = \frac{\partial(\Delta G^{e}/k_{B}T)}{\partial n_{L}} = \frac{1}{r_{c}}\left[\alpha_{e}\Phi_{0}^{2/3}\phi_{P}^{1/3} - \frac{3}{f}(\Phi_{0}^{2/3}\phi_{P}^{4/3} - \phi_{P}^{2}) - \beta_{e}(1 + \ln \phi_{P})\right] \tag{22}$$

Substituting eqs 19, 20, and 21 into eq 18 for the case where $\alpha_e$ and $\beta_e$ are independent of $\phi_P$, the equilibrium condition is given by the following equation

$$\left\{\ln \phi_{L} + (1 - \phi_{L}) + \chi(1 - \phi_{L}^{2}) - \ln z + {}^1/_2\nu\phi_{L}^{2}s^{2} + \frac{(1 - \phi_{L})}{r_{c}}[\alpha_{e} - \beta_{e}]\right\}^{I} = \{-\ln z + {}^1/_2\nu s^{2}\}^{II} \tag{23}$$

Similarly, substituting eqs 19, 20, and 22 into eq 18 for the case where $\alpha_e$ and $\beta_e$ depend on $\phi_P$, the resulting equation is

$$\left\{\ln \phi_L + (1 - \phi_L) + \chi(1 - \phi_L^2) - \ln z + {}^1/_2\nu\phi_L^2 s^2 + \frac{1}{r_c}[\alpha_e(1 - \phi_L) - \beta_e(1 + \ln(1 - \phi_L))]\right\}^I = \{-\ln z + {}^1/_2\nu s^2\}^{II} \quad (24)$$

When the LC is in the isotropic state at some $T > T_{NI}$ or $\phi_L < \phi_{L,c}$ such that nematic ordering is prohibited,[9] the term $(-\ln z + {}^1/_2\nu\phi_L^2 s^2)$ on the left-hand side of both eqs 23 and 24 would drop out. In this situation, one obtains the familiar equation for the equilibrium swelling of an isotropic network by an isotropic solvent.[20,21,27] Thus, in the analysis of swelling of an isotropic network by a nematic LC solvent, one must incorporate the contribution of the LC ordering potential as it is an integral part of the equilibrium equation, particularly at $T < T_{NI}$ and $\phi_L > \phi_{L,c}$.

**Numerical Calculation.** Given $T_{NI}$, $r_c$ ($r_L = 1.0$), and $f$, the volume fraction, $\phi_L^I$, of the LC in the swollen network (phase I) which is in equilibrium with a pure solvent (nematic or isotropic) may be calculated for a specified temperature, $T$, either from eq 23 or 24. Notice that the term on the right-hand side of eqs 23 and 24 is independent of $\phi_L$, but it could vary with $T$ since $z$ and $s$ are both functions of $T$ (see Figure 1). However, the left-hand side of both equations is evaluated at $\phi_L = \phi_L^I$ at each $T$. Thus, $\phi_L^I$ is the only unknown parameter in either equations. All other parameters necessary to evaluate $\phi_L^I$ numerically are either known or could be calculated from other known parameters. For example, when $f$ is given, $\alpha_e$ and $\beta_e$ are known. Similarly, once the $T_{NI}$ is specified, it allows the calculation of $\nu$, $z$, and $s$ at any $T$, and since $T$ is given, $\chi$ can be computed according to eq 5. To estimate $\phi_L^I$, eqs 23 and 24 were solved self-consistently using the Newton−Raphson iterative scheme. In the numerical calculations, Simpson's numerical integration procedure was used in solving the integrals defining $z$ and $s$.

We have calculated coexistence swelling curves in order to examine the effects of $r_c$, $f$, and volume fraction $\phi_P$ (or $\phi_L$) dependence of network constants $\alpha_e$ and $\beta_e$. The calculated phase diagrams of nematic LC/cross-linked flexible polymer were compared with those of nematic LC/monomer and LC/linear polymer systems. The theoretical phase diagrams of LC/monomer and LC/polymer mixtures were established following the procedure of Shen and Kyu.[9] For the detailed procedure, interested readers are referred to the original paper of Shen and Kyu.[9]

Finally, the theoretical predictions have been tested with the experimental phase diagrams of the mixture of low molar mass single-component nematic liquid crystal, i.e., 4-*n*-heptyl 4′-cyanobiphenyl (K21, $T_{NI} = 42$ °C) and in-situ photo-cross-linked multifunctional thiolene-based optical adhesive (NOA65).

## Experimental Section

**Materials.** K21 nematic liquid crystal (LC) was purchased from BDH Chemicals (a subsidiary of Merck), Poole, England. K21 has a crystal−nematic transition ($T_{KN}$) of 28.5 °C and nematic−isotropic transition ($T_{NI}$) of 42 °C. UV-curable thiolene-based optical adhesive (NOA65) was purchased from Norland Products Inc., New Brunswick, NJ. NOA65 has a density[12] of 1.12 g/cm$^3$ and a maximum absorption[34] in the 350−380 nm wavelengths. Both K21 and NOA65 were used as received without further purification.

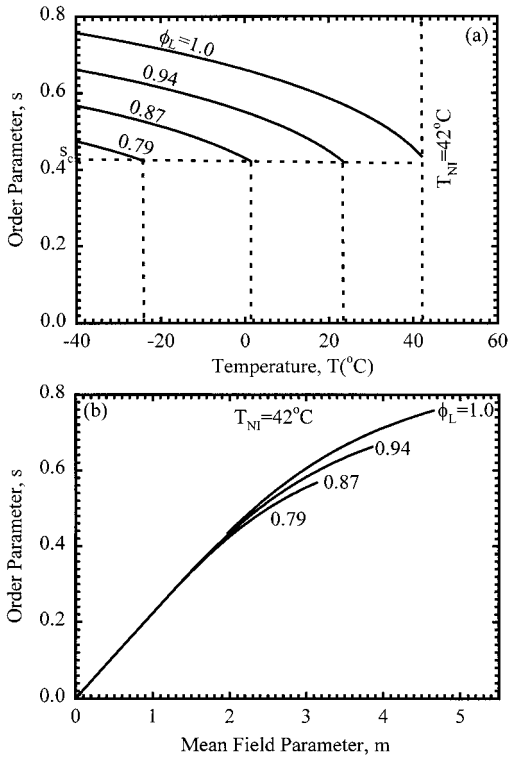


**Figure 1.** Order Parameter, $s$, as a function of temperature, $T$ (a), and mean field parameter, $m$ (b), at selected nematic LC volume fractions, $\phi_L$.

**Establishment of LC/Monomer Phase Diagram.** Smith[12] reported that there are four primary constituents in the uncured NOA65 such as trimethylolpropane diallyl ether, trimethylolpropane tris thiol, isophorone diisocyanate ester, and benzophenone photoinitiator. Except for the benzophenone photoinitiator whose concentration is about 5 wt %, the concentrations of other components were not disclosed.[34] Smith[13] further reported that uncured NOA65 is a mixture of monomers and oligomers, though the ratio of monomers to oligomers is not given. The molecular weight (400 g/mol) of the uncured NOA65 suggests that the amount of oligomers is probably very small.[34] Hence, the uncured NOA65 may be assumed to contain mainly monomers. In the establishment of K21/uncured NOA65 phase diagram, we shall therefore treat the system as a pseudobinary mixture.

The LC/monomer phase diagram was established by means of polarized optical microscopy and light scattering. Mixtures for the establishment of LC/monomer phase diagram were prepared by weighing appropriate amounts of NOA65 and K21 in small vials and then thoroughly shaken (without any solvent) to achieve intimate mixing. Samples were sandwiched between micro-glass slides yielding a thickness range of 10−20 $\mu$m. The samples were stored in the refrigerator in the dark and handled under dimmed room light to prevent any unwarranted photopolymerization-induced phase separation.

For the optical microscopy experiment, a Nikon Optipot 2-POL microscope with a filtered Halogen light source (12 V, 100 W) was used. Lens magnification was 400×. Pictures were taken using photographic attachments composed of a Nikon FX-35DX camera connected to a Nikon UFX-DX exposure controller. For sample heating and cooling, a Linkam Scientific Instruments sample stage (model TS1500) connected to a Linkam programmable temperature controller (model TMS93) and a cooling system (model LNP93/2) was used. Samples were heated until optically clear, cooled slowly, and then observed under the microscope for any phase change. Thereafter, they were reheated again to the isotropic state. The heating and cooling rate was 1 °C/min.

For the light scattering experiment, a randomly polarized He−Ne laser light source (2 mW, Aerotech, model LSR2R) with

a wavelength of 632.8 nm was used. Cloud points were measured by monitoring a sudden change of the scattered intensity at a fixed angle (~10°) using a photodiode detector (Hamamatsu Co., model HC-220-01). A sample stage coupled with a programmable temperature controller (Omega, model CN-2012) with a resolution of ±0.1 °C was utilized. The temperature scans were performed at a rate of 1 °C/min for both cooling and heating. A personal computer and an A/D converter were linked to the light-scattering setup for data acquisition and storage.

**Preparation of LC/Photo-Cross-Linked Polymer Composite.** Various uncured samples were placed on transparent micro-glass slides covered with thin transparent circular glasses for thickness uniformity. These samples yielding a thickness range of 10−20 $\mu$m were photo-cross-linked isothermally under the microscope at 40 °C for 10 min in order to fabricate LC/cross-linked polymer composites. At 40 °C, most LC/monomer mixtures were in the isotropic phase, except for extremely high LC compositions (see Figure 1 in ref 15). The photo-cross-linking was done using a UV curing unit (model ELC403, Electrolite Corp.). The instrument output was 40 mW/cm$^2$ in the 350−380 nm wavelengths. An exposure time of 5 min was recommended for the neat (100%) NOA65 to achieve a full conversion.[34] However, the LC/monomer blends were irradiated for 10 min to ensure full conversion for high LC mixtures. We refer interest readers to our previous paper[15] on photopolymerization behavior including the temporal dependence of conversion. The composites thus prepared consisted of phase-separated nematic LC droplets in a matrix of cross-linked NOA65.

In the comparison between the theoretical phase diagram and the experimental observation for the K21/cross-linked NOA65 system, various parameters such as linear segment length ($r_P$), segment length between cross-links ($r_c$), and functionality ($f$) of the network were considered. The gross molecular weight (related to $r_P$) and molecular weight between cross-links (related to $r_c$) in principle may be estimated roughly through stoichiometry. However, it should be cautioned that the starting material is a mixture of multifunctional monomers and oligomers,[12] some of which are difunctional. Hence, it can be anticipated that the network structure must be very complex and the actual molecular weights may be at variance with the simple estimation afforded by the stoichiometry approach. Moreover, it is by no means easy to determine $r_p$ and $r_c$ themselves experimentally, particularly in the presence of anisotropic LC solvent (see the phase diagram in ref 15). Ignoring possible effects of variations in structure and varying molecular weights, the LC/cross-linked polymer system may be treated as a pseudobinary mixture composed of K21 and photo-cross-linked NOA65. The $r_p$ and $r_c$ values (i.e., 10, 100, and 150) were chosen arbitrarily to demonstrate the predictive capability of theory in comparing the experiment. It should be pointed out that the values of $r_p$ and $r_c$ used are within the range used by Benmouna et al.[18,19] and Bauer et al.[20,21] in their studies. Also, since NOA65 contains bifunctional monomers, some linear chain propagation can be anticipated during the network formation, which undoubtedly makes the network more flexible.

Regarding network average functionality $f$, based on thiolene chemistry, trimethylolpropane diallyl ether and isophorone diisocyanate ester are both bifunctional; only trimethylolpropane tris thiol is trifunctional. Since uncured NOA65 is known to cross-link[12,13,15,35] upon irradiation with UV light, it is reasonable to assume that the polymer network has an average functionality, $f = 3$ (if the uncured NOA65 contains mainly trimethylolpropane tris thiol). Note that $f = 3$ is the minimum functionality required for network formation during the cross-linking reaction. It was further assumed that the photo-cross-linked NOA65 ($f = 3$) obeys the Flory[30] affine network model.

**Establishment of LC/Cross-Linked Polymer Phase Diagram.** The LC/cross-linked polymer phase diagram was experimentally established using optical microscopy. LC/cross-linked polymer networks prepared as described above were subjected to the heating and cooling cycles at a rate of 1 °C/min. Since the phase transition is thermally reversible, the phase transition temperature can be determined in the microscopic investigation by repeating the heating and cooling cycles in a small temperature gap near the transition temperature while recording all images on the computer with the aid of the CCD camera and image analyzer. Also, micrographs were taken to illustrate the coexistence regions.

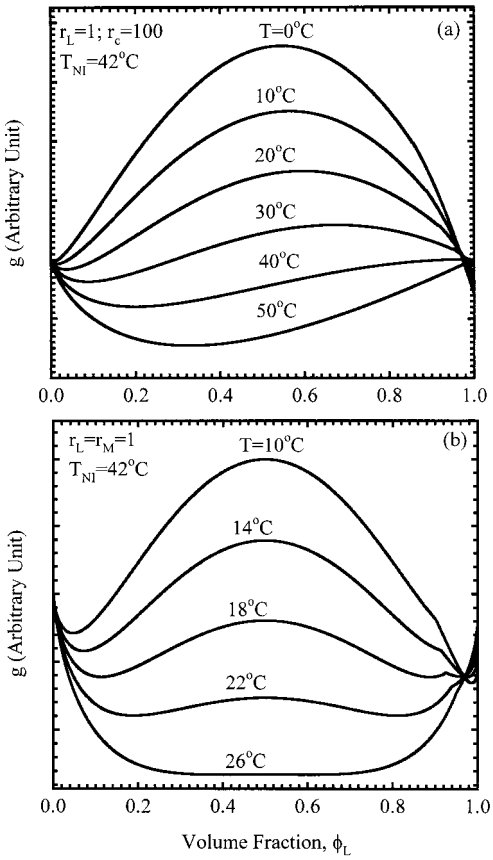


**Figure 2.** Free energy density, $g$, vs volume fraction, $\phi_L$, for the nematic LC/polymer network system (a) in comparison with that of nematic LC/monomer (b).

## Result and Discussion

**Order Parameter.** It is of interest to first examine the behavior of order parameter, $s$, as a function of temperature, $T$, volume fraction, $\phi_L$, and mean field parameter, $m$. For a given $T$ and $\phi_L$, $s$ can be obtained by simultaneously solving eqs 8, 9, and 10. Figures 1a depicts $s$ as a function of $T$ at selected $\phi_L$, while Figure 1b shows $s$ as a function of $m$ for the same $\phi_L$. For a given $T$, there exists a critical order parameter, $s_c$, with a corresponding volume fraction, $\phi_{L,c}$ above which a stable nematic phase can exist.[9] At $s_c$, the order parameter drops sharply to zero, indicative of a first-order transition. It is important to note that the behavior of $s$ depicted in Figure 1a,b is unaffected by the presence of cross-links in the network. This finding is not surprising in view of the fact that the anisotropic free energy of Maier−Saupe theory is applicable regardless of topology (linear or cross-linked) of the polymer.[9] Thus, for a given $T$ and $\phi_L$, $s$ depends only on the $T_{NI}$ of the nematic LC.

**Free Energy of Nematic LC/Polymer Network System.** Next, we examine the variation of free energy density, $g$, of nematic LC/cross-linked polymer system vs LC volume fraction, $\phi_L$. Figure 2a shows such plots for selected temperatures for a polymeric network

having an repeat unit between cross-links, $r_c$, of 100 and obeying Flory affine network model[30] ($f = 3$; $\alpha_e$ and $\beta_e$ independent of $\phi_L$ or $\phi_P$). For reference, a set of $g$ vs $\phi_L$ curves for the LC/monomer mixture is shown in Figure 2b.

As can be seen in Figure 2a, only one minimum exists in each curve associated with the stable isotropic swollen network (isotropic gel). The behavior in Figure 2a may be contrasted to that of Figure 2b for the LC/monomer system or even for the LC/linear polymer system[9] in which at least two minima are normally seen depending on temperature. The reason for the observed single minimum in Figure 2a implies that the polymer network can no longer be dissolved in the anisotropic LC solvent; i.e., no minimum is observable in the LC-rich region ($\phi_L \rightarrow 1$). However, the LC can be dissolved and incorporated in the network via swelling; hence, it is usual to observe the minimum in the network-rich region ($\phi_L \rightarrow 0$).

It should be pointed that the trend in $g$ vs $\phi_L$ curves depends not only on the network model type, $r_c$, and $T_{NI}$ (hence $\nu$) used but also on the dependence of $\chi$ on $T$. In our calculations for LC/polymer network system, we have utilized the $\chi$ values obtained for the LC/monomer system, since our network was made in situ in the presence of LC.

**Phase Behavior: LC/Cross-Linked Polymer vs LC/Linear Polymer.** In previous studies,[15,35] we investigated the influence of LC/monomer phase behavior on the reaction kinetics[15] and emergence of morphology[35] during photopolymerization of the K21/NOA65 system. In this paper, we shall extend our study to theoretical and experimental investigations of phase diagrams of the mixture of nematic LC (K21) and photo-cross-linked network (NOA65).

It can be anticipated that the topological differences of polymers such as linear chains vs cross-linked networks would influence the phase diagram of the nematic LC/polymer system. To demonstrate this effect, the phase diagrams of LC with a cross-linked polymer have been calculated self-consistently based on the network model of Flory[30] and subsequently compared with that of the LC/linear polymer. For the purpose of comparison, $r_p$ is taken to be equal to $r_c$. The calculated phase diagrams are depicted in parts a and b of Figure 3, along with that of the initial LC/monomer system. The phase diagram of the LC/monomer system is typically an upper critical solution temperature (UCST) overlapping with a narrow isotropic + nematic coexistence region associated with the nematic ordering.[9,15] It normally shows two coexisting phases except at the eutectic point (delineated by a dotted horizontal line) where three phases can coexist.

Linear or cross-linking polymerization generally widens the immiscibility gap of the LC/polymer mixture due to an increase in molecular weight of the polymerizing component. When the segment length of a linear polymer, $r_P$, increases from 10 to 100, the miscibility between the nematic LC and the linear polymer gets poorer, thereby raising the UCST coexistence curve to a higher temperature (Figure 3a). The $T_{NI}$ of the neat LC and/or of the LC-rich compositions remain unchanged, while the I + N and I + I coexistence regions get smaller. When the segment length (molecular weight) between the cross-link points, $r_c$, changes from 100 to 10 due to the cross-linking, the network becomes tighter, and it also reduces the miscibility of the nematic

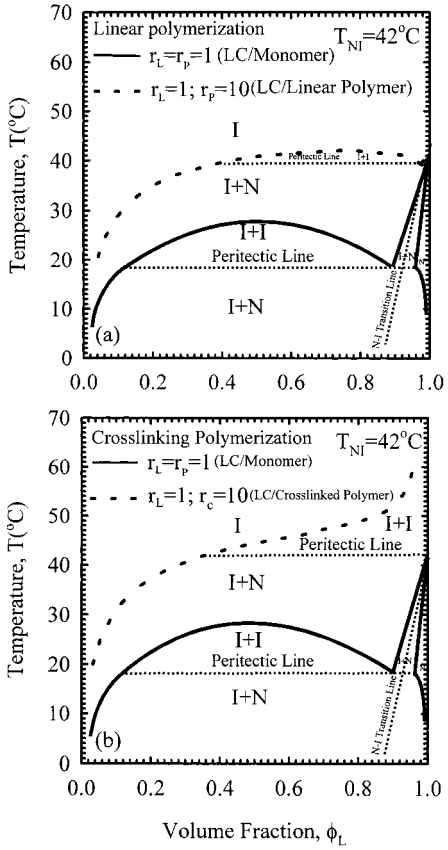


**Figure 3.** Comparison of theoretical phase diagrams for mixtures of nematic LC/linear polymer (a) with nematic LC/cross-linked polymer (b) calculated using the indicated parameters. The theoretical phase diagram of the LC/monomer system is also included in the figure for reference.

LC/cross-linked polymer mixture. Consequently, the coexistence curve moves to a higher temperature (Figure 3b). The coexistence curve makes an upward turn in the LC-rich region ($\phi_p \rightarrow 1$) due to the domination by the network elastic free energy.

Unlike the LC/linear polymer phase diagram, the LC/cross-linked polymer phase diagram shows no discernible critical point (Figure 3b). The absence of a critical point is again due to the domination of the elastic free energy of the network in the free energy expression of the LC/polymer network system. In other words, the regular entropy of mixing term $(\phi_P \ln \phi_P)/r_P$ of the polymer has been replaced by the elastic free energy of the network, which is entropic in origin. In both systems, however, the free energy density of nematic ordering remains unchanged. When the network is formed, it can no longer be dissolved in the pure LC. Flory[36] and de Gennes[37] recognized long ago that polymer networks are highly incompatible with nematic solvents. As a consequence, the binodal curves of LC/cross-linked polymer network exhibit an upward change in curvature as the volume fraction, $\phi_L$, of LC approaches unity. At low values of $\phi_L$ (i.e., network-rich region), one can readily see that the binodal curves for LC/linear polymer and LC/cross-linked polymer systems behave almost the same. It is reasonable to infer that the free energy due to network elasticity is the main reason for the observed difference between the thermodynamic properties of the LC/cross-linked network and that of the LC/linear polymer systems.

**Effect of Segment Length between Cross-Links on Phase Diagrams.** The segment length between

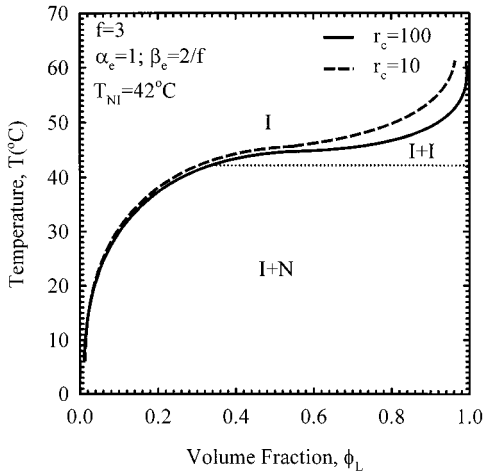


**Figure 4.** Effect of the average size of the segment length between cross-linked points, $r_c$, on calculated phase diagrams of mixtures of nematic LC and cross-linked polymer network.

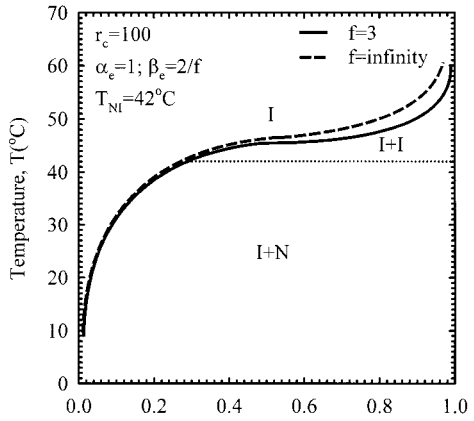


**Figure 5.** Effect of network functionality, *f*, on the calculated phase diagrams of mixtures of nematic LC and cross-linked polymer ($f = 3$ represents the Flory affine network model, whereas $f = \infty$ represents James and Guth phantom network model).

cross-linked points, $r_c$, is a measure of cross-link density relating to the elasticity of a polymer network. It is of interest to examine the influence of $r_c$ on the miscibility between an LC solvent and a flexible chain polymer network. Figure 4 depicts the calculated phase diagram illustrating the effect of molecular segment lengths between the cross-linked points, $r_c$, on the coexistence curves. The nematic−isotropic (N−I) transition temperature is taken to be that of the single-component K21 liquid crystal, i.e., 42 °C. The polymeric network is assumed to have a functionality of 3 and also obeys the Flory model,[30] but with different segment length between cross-linked points ($r_c = 10$ or 100).

Considering one of the curves, say the case $r_c = 100$, the coexistence curve gives the composition of the swollen network in equilibrium with a continuum of liquid crystal solvent (Figure 4). The LC solvent may be either in the nematic ($T < T_{NI}$) or in the isotropic region ($T > T_{NI}$). The dotted horizontal line shows the $T_{NI}$ of the LC. In the phase diagram of the LC/polymer network, the free energy contribution of the swollen network dominates in the high LC region, giving rise to the coexistence curve showing an upward turn asymptotically toward the axis of the pure LC. This is because elasticity suppresses excessive swelling which results in phase separation between the swollen network and the pure solvent.

Three regions may be identified in the descending order of temperature, i.e., isotropic gel (I) or swollen network, isotropic network + isotropic solvent (I + I), and isotropic network + nematic solvent (I + N). There is little or no effect of the network elasticity on the coexistence curve in the low LC region ($\phi_L \rightarrow 0$) below the $T_{NI}$, but the effect of network elasticity is significant in the high LC region ($\phi_L \rightarrow 1$) above the $T_{NI}$. With increasing $r_c$, the isotropic network−isotropic solvent (I + I) region gets smaller, while the coexistence curve shifts asymptotically to the high LC content side. Another interesting observation in Figure 4 is that the I + I transition is more sensitive to changes in $r_c$ than the I + N region.

In Figure 4, it is apparent that a more flexible network with $r_c$ of 100 at a given temperature can accommodate solvent relative to a less flexible (denser) one with $r_c$ of 10. This is why the binodal curve for $r_c = 10$ appears steeper than that for $r_c = 100$, and it tends to moves away from the $\phi_L = 1$ axis.

**Effect of Network Functionality.** One can also anticipate that phase behavior of the blends of nematic LC and cross-linked flexible chain polymer would depend on the network functionality or topology because a large *f* corresponds to a tight or a dense network, whereas a small *f* signifies a loose network. Figure 5 depicts the calculated coexistence curves for a Flory affine network[30] ($f = 3$) in comparison with that of James and Guth phantom network[31] ($f = \infty$) with $r_c = 100$ in both cases. Both models assume that the network parameters, $\alpha_e$ and $\beta_e$, are independent of $\phi_P$. In comparison with the phantom network for the same $r_c$, the affine network is apparently swollen more by the LC solvent in both the isotropic and the nematic regions. This may be attributed to the fact that the larger the functionality, the larger the number of arms at a given cross-linked point. Hence, a network with multiple (four or more) arms would be tighter than a two- or three-arm network.

Qualitatively speaking, the effect of *f* on the phase diagrams (Figure 5) shows a similar trend to that of $r_c$ (Figure 4). This should be expected since the two effects are complementary. However, the effect of *f* on a network having a fixed $r_c$ on the phase diagram (Figure 5) is less pronounced relative to that of $r_c$ for a network having a fixed *f* (Figure 4), particularly above the $T_{NI}$ where the LC is isotropic. Below the $T_{NI}$ in the region $\phi_L \rightarrow 0$, the effects of $r_c$ and *f* do not show any significant difference.

**Effect of $\phi_L$ (or $\phi_P$) Dependence of Network Model Parameters ($\alpha_e$ and $\beta_e$).** Next, we examined the effect $\phi_L$ (or $\phi_P$) dependence of network model parameters ($\alpha_e$ and $\beta_e$ on the phase behavior of the nematic LC/cross-linked network. Comparison has been made between the calculated curves based on the affine model of Flory[30] and that of Petrovic et al.[32] In the former case, $\alpha_e$ and $\beta_e$ of the network are independent of $\phi_P$, while in the latter case a linear dependence of $\alpha_e$ and $\beta_e$ on $\phi_P$ is assumed. Figure 6a shows the calculated curves for these two network models having $f = 3$ and $r_c = 100$. Figure 6b shows an enlarged version of the plot between $\phi_L = 0.8$ and $\phi_L = 1.0$. Although the model of Petrovic et al.[32] reveals a slightly smaller swelling behavior relative to that of the Flory affine[30] network (as $\phi_L \rightarrow 1.0$ or $\phi_P \rightarrow 0$), the two models show essentially a similar trend. In other words, imposing a linear dependence of $\alpha_e$ and $\beta_e$ on $\phi_P$ has very little effect on

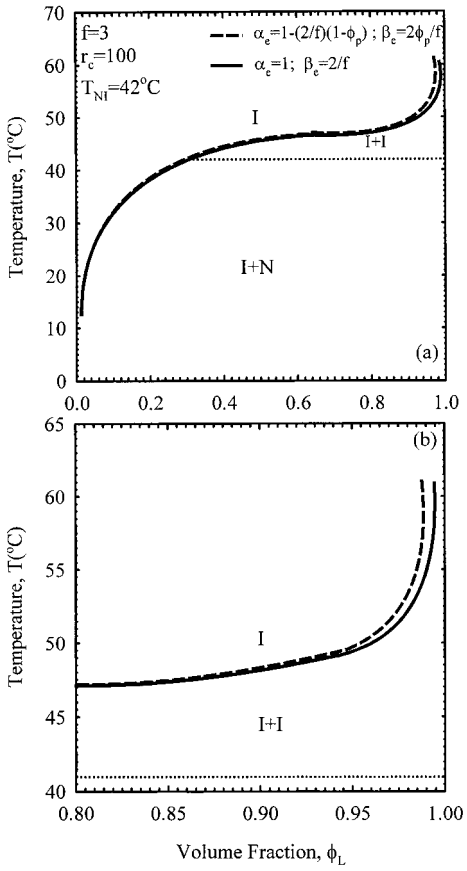


**Figure 6.** Effect of volume fraction, $\phi_L$, dependence of the network model parameters, $\alpha_e$ and $\beta_e$, on calculated the phase diagrams of the nematic LC/cross-linked polymer system.

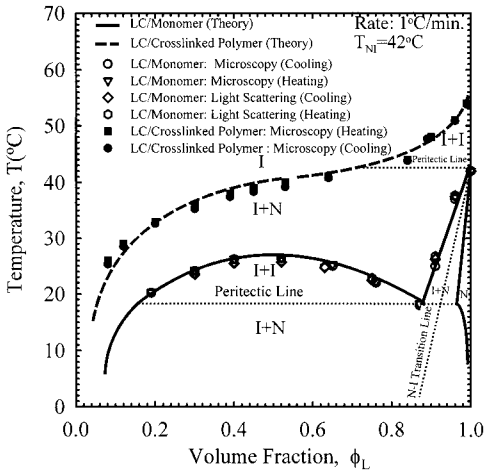


**Figure 7.** Experimental phase diagrams of K21/photo-cross-linked NOA65 in comparison with theory. Included in the figure for reference are the corresponding phase diagrams of the K21/uncured NOA65 system.

the phase behavior, provided all other parameters are kept constant. Boots et al.[17] reached a similar conclusion from their conversion-phase diagram calculations.

**Test of Theory with Experimental Phase Diagrams.** To test the validity of theoretical predictions, we experimentally established the phase diagram of the K21/photo-cross-linked NOA65 system. Figure 7 shows the experimental phase diagram of LC/cross-linked polymer in comparison with the theory. Also included is the observed phase diagram of the LC/monomer system from our earlier paper.[15]

In Figure 7, one can recognize a remarkable fit between theoretical prediction and the transition temperatures obtained for heating and cooling cycles by the various methods used. Note that for the LC/monomer and LC/polymer systems the temperatures for the N + I to I + I transitions delineated by the dotted horizontal lines were not measured experimentally but were drawn based on the theoretical prediction. The various coexistence regions of the LC/monomer and LC/cross-linked polymer phase diagram were identified by optical microscopy and labeled accordingly for each system.

The uncured NOA65 has been assumed to have an average functionality, *f*, of 3, i.e., an idealized polymer network obeying the Flory affine network model.[30] The segment length between cross-linked points of the photo-cross-linked NOA65 was not measured because of the complex solubility behavior of anisotropic LC solvent in the network. Instead, $r_c$ of 150 was simply used to fit the experimental data. It is apparent in Figure 7 that there is a good qualitative agreement between the theory and the experiment, attesting to the reasonable predictive capability of the theory.

In regards to the LC/cross-linked polymer phase diagram, the predicted coexistence regions have been identified by means of optical microscopy by monitoring LC ordering transition in competition with phase separation. Figure 8 shows the optical micrographs for the 90/10 K21/photo-cross-linked NOA65 network. The composite network was prepared by photo-cross-linking of an initially miscible K21/NOA65 mixture at 40 °C. The photo-cross-linking reaction induces instability in the system, which drives the system to phase separate. The phase-separated nematic LC domains grow via coalescence until the growth is restricted by the network. This process is known to occur very fast.[14,15,35] After photo-cross-linking, the morphology of these composites reveals phase-separated polygonal-shaped nematic LC droplets dispersed in a matrix of cross-linked NOA65. It is worthy to mention that this type of morphology (Figure 8) has been observed for LC/photo-cross-linked acrylate system by Amundson et al.[38] using confocal microscopy.

It should be emphasized that the LC/network blend can still undergo swelling and deswelling. Recall that the N−I transition temperature of K21 is 42 °C. Above 50 °C, the domain boundaries are discernible, as the network cannot be dissolved in the anisotropic solvent. The isotropic LC molecules are presumably dissolved in the network during swelling. The network may be regarded as being swollen to saturation by the solvent. In Figure 7 the 90/10 mixture at 50 °C is considered to be in the isotropic swollen network or gel (I) region. We confirmed that the network remains intact during continued heating of the sample well above 50 °C. Further, the LC were removed by immersing the samples in *n*-heptane for 2 days and washed several times.[35] The resulting network structures were found to be similar[35] to the original one.

Upon cooling to 45 °C, i.e., below the binodal curve (see Figure 7), deswelling takes place in which some isotropic LC droplets appear within the swollen network (isotropic gel), indicating the coexistence of isotropic network + isotropic solvent (I + I). As the temperature is further lowered to below the $T_{NI}$ (42 °C), the swollen network deswells further leading to nematic ordering as shown in the picture at 39 °C. With continued cooling to 36 °C, a Schlieren texture as typical for nematic LC

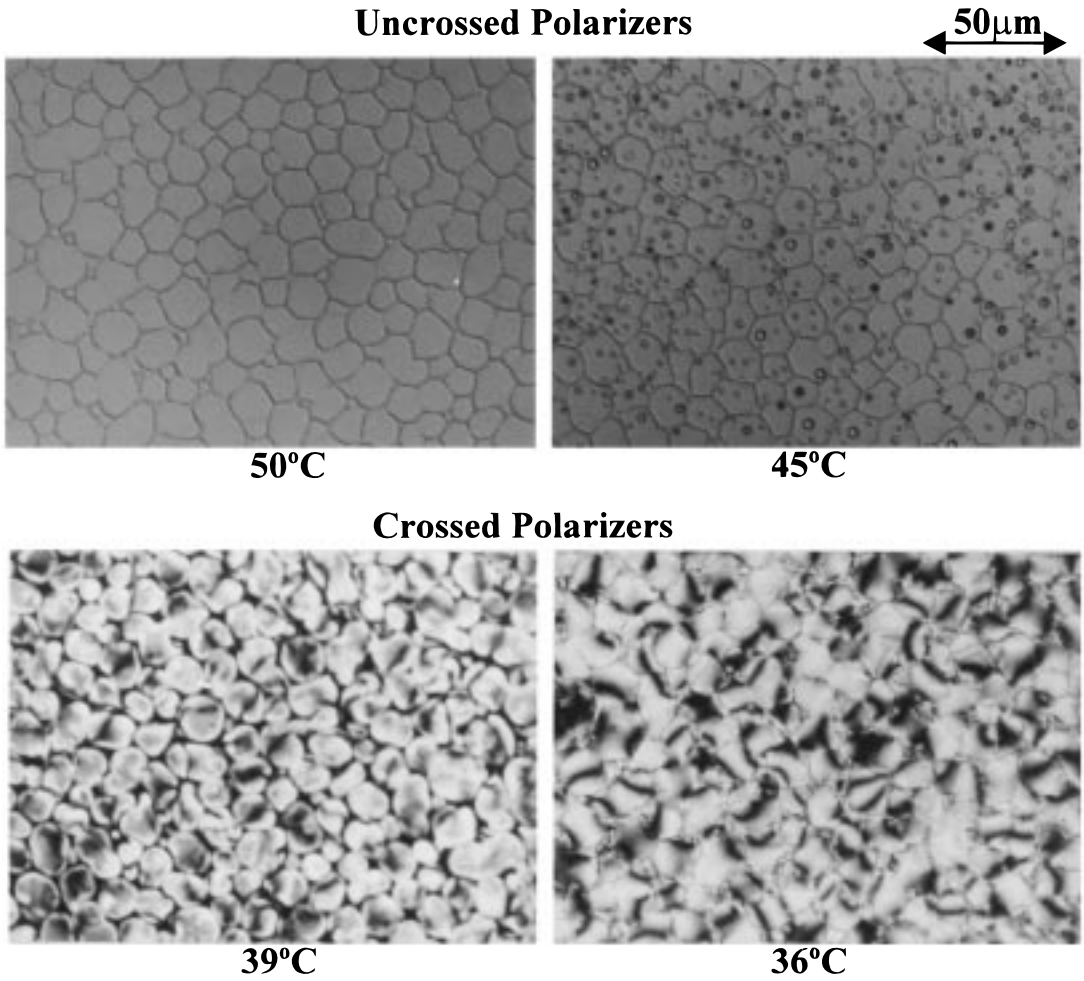


**Figure 8.** Optical micrographs showing the coexistence regions identified for 90/10 K21/photo-cross-linked NOA65 composite. The optical micrographs represent various coexistence regions such as isotropic gel (I) at 50 °C, isotropic network + isotropic solvent (I + I) at 45 °C, and isotropic network + nematic solvent (N + I) at 39 and 36 °C. Cooling rate was 1 °C/min.

defects can be discerned under crossed polarizers, indicating the coexistence of isotropic network + nematic solvent (I + N).

To examine how the coexistence regions vary with the liquid crystal (K21) concentration, Figures 9 and 10 respectively show the optical micrographs of the regions identified for the 85/15 and 60/40 compositions. These composites were prepared in the same way and subjected to the same thermal treatment as the 90/10 composite. The same behavior, i.e., the coexistence regions observed for the 90/10 composite, can be identified in the 85/15 blend (Figure 7). However, when the concentration of K21 is further reduced to 60 wt %, only two coexistence regions were discerned: isotropic gel (I) and isotropic network + nematic (I + N) coexistence regions. The isotropic network + isotropic solvent (I + I) region is absent in the 60/40 composition. As one can see in Figure 7, the isotropic network + isotropic (I + I) region decreases as the volume fraction of LC decreases as predicted by the theory. It should be emphasized that the I + I and the I + N regions as identified experimentally is strictly for a pseudo-two-phase system since one cannot rule out the possible presence of unreacted monomers and oligomers, short (cyclic) polymer chains, and residual photoinitiator in the cured mixtures. It is believed the amount of these species is very small relative to the amount of LC solvent given the fast nature of the photo-cross-linking reaction.[15] Nevertheless, we are able to verify experimentally the predicted phase diagram as well as the coexisting phases of mixtures of nematic LC and in-situ photo-cross-linked isotropic polymer network.

## Conclusions

In this paper, we have combined the free energy of isotropic mixing, nematic ordering, and elasticity in describing the thermodynamic phase behavior of nematic LC/cross-linked polymer system. Calculations were carried out self-consistently in establishing various phase diagrams as functions of segment between cross-linked points ($r_c$), network functionality ($f$), and the network parameters ($\alpha_e$ and $\beta_e$). Each calculated phase diagram captured three coexistence regions: isotropic gel (swollen network), isotropic network + isotropic solvent, and isotropic network + nematic solvent coexistence regions. It was found that decreasing statistical segment length ($r_c$) or increasing functionality ($f$) leads to a tighter (denser) network. As compared to a looser network, the tighter network swells less in the LC solvent. It was found that the effect of varying $r_c$ on the calculated phase diagrams was more pronounced than the effect of varying $f$. There is only a minor difference in the coexistence curves for the various network models considered, i.e., whether the network parameters $\alpha_e$ and $\beta_e$ are $\phi_P$-dependent or not.

A comparison was made between the phase diagrams of LC/linear polymer and LC/cross-linked polymer sys-

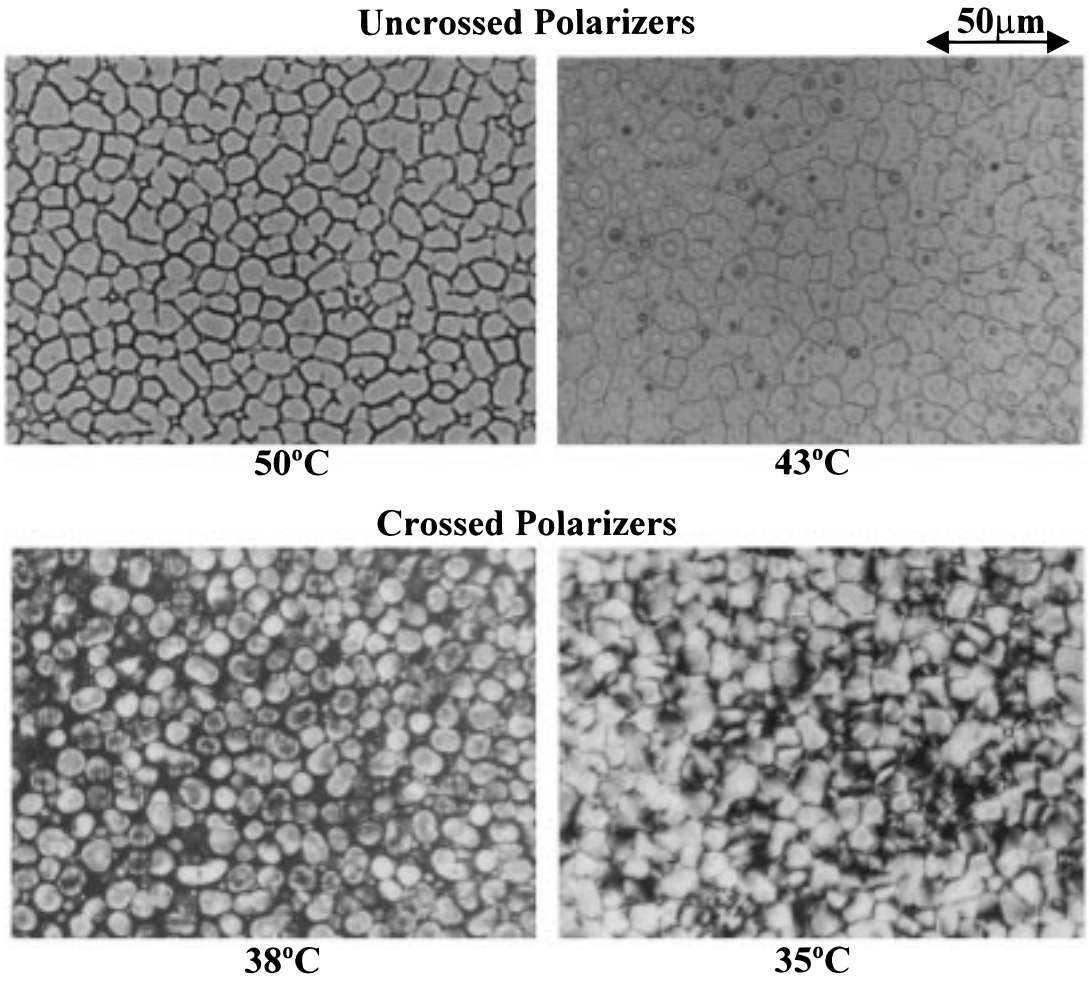


**Figure 9.** Optical micrographs showing the coexistence regions observed for the 85/15 K21/photo-cross-linked NOA65 composite. The pictures represent various coexistence regions including isotropic gel (I) at 50 °C, isotropic network + isotropic solvent (I + I) at 43 °C, and isotropic network + nematic solvent (N + I) at 38 and 35 °C. Cooling rate was 1 °C/min.

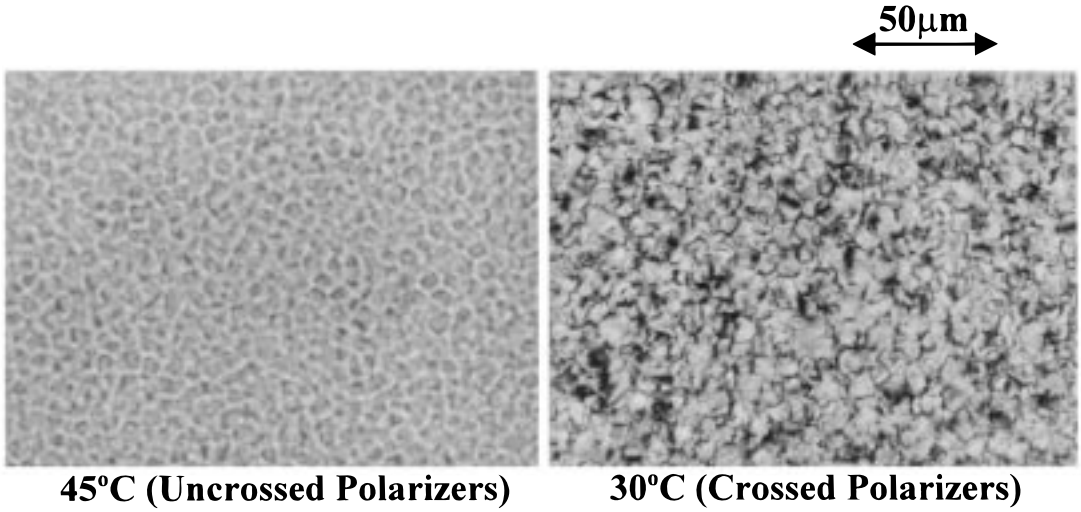


**Figure 10.** Optical micrographs showing the coexistence regions observed for the 60/40 K21/photo-cross-linked NOA65 composite. The micrographs represent the coexistence regions such as isotropic gel (I) at 45 °C and isotropic network + nematic solvent (N + I) at 30 °C. Cooling rate was 1 °C/min.

tems. In general, linear polymerization (increasing $r_P$) or cross-linking reaction (decreasing $r_c$) leads to a widening of the immiscibility gap within the phase diagram of the LC/polymer mixture. Another interesting feature is that there is no critical point in the LC/cross-linked polymer phase diagrams unlike those of LC/linear polymer. This is due to the domination of the elastic free energy of the polymer network. Another consequence of the network elasticity is that when the volume fraction of LC approaches unity, the binodal curve of LC/cross-linked polymer system undergoes an upward turn in curvature. In the lower range of $\phi_L$, no significant difference was seen. Finally, we able to verify the predicted phase diagram and coexistence regions for

the K21/photo-cross-linked NOA65 system. A remarkably good agreement between theory and experiment was obtained.

**Acknowledgment.** Support of this work by the NSF-STC Center for Advanced Liquid Crystal Optical Materials (ALCOM) via Grant No. 89-20147 is gratefully acknowledged. We are indebted to H.-W. Chiu for his critical comments and suggestions.

## References and Notes

(1) Drzaic, P. S. *Liquid Crystal Dispersions*; World Scientific: Singapore, 1995.
(2) Doane, J. W. In *Liquid Crystal: Applications and Uses*; Bahadur, B., Ed.; World Scientific: Singapore, 1990; Chapter 14, p 361.
(3) Montgomery, G. P.; Smith, G. W.; Vaz, N. A. In *Liquid Crystalline and Mesomorphic Polymers*; Shibaev, V. P., Lam, L., Eds.; Springer: New York, 1994; Chapter 5, p 149.
(4) Isayev, A.; Kyu, T.; Cheng, S. Z. D., Eds. *Liquid Crystalline Polymer Systems: Technological Advances*; ACS Symposium Series 632; American Chemical Society: Washington, DC, 1996.
(5) Crawford, G. P., Zumer, S., Eds. *Liquid Crystals in Complex Geometry Formed by Polymer and Porous Networks*; Taylor and Francis: London, 1996.
(6) Paleous, C. M., Ed. *Polymerization in Organized Media*; Gordon and Breach: Philadelphia, 1992.
(7) West, J. L. *Mol. Cryst. Liq. Cryst.* **1988**, *157*, 427.
(8) Ahn, W.; Kim, C. Y.; Kim, H.; Kim, S. C. *Macromolecules* **1992**, *25*, 5002.
(9) Shen, C.; Kyu, T. *J. Chem. Phys.* **1995**, *103*, 7471.
(10) Kyu, T.; Chiu H.-W. *Phys. Rev. E* **1996,** *53*, 3618.
(11) Kyu, T.; Ilies, I.; Shen, C.; Zhou, Z. L. In ref 4.
(12) Smith, G. W. *Mol. Cryst. Liq. Cryst.* **1991**, *196*, 89.
(13) Smith, G. W. *Phys. Rev. Lett.* **1993,** *70*, 198.
(14) Serbutoviez, C.; Kloosterboer, J. G.; Boots, H. M. J.; Touwslager, F. J. *Macromolecules* **1996**, *29*, 7690.
(15) Nwabunma, D.; Kim, K.-J.; Lin, Y.; Chien, L.-C.; Kyu, T. *Macromolecules* **1998**, *31*, 6806.
(16) Hirai, R.; Niiyama, S.; Kumai, H.; Gunjima, T. *Proc. SPIE-Int. Soc. Opt. Eng.* **1990,** *1257*, 2; *Rep. Res. Lab., Asahi Glass Co., Ltd.* **1990**, *40*, 285.
(17) Boots, H. M. J.; Kloosterboer, J. G.; Serbutoviez, C.; Touwslager, F. J. *Macromolecules* **1996**, *29*, 7683.
(18) Benmouna, F.; Bedjaoui, L.; Maschke, U.; Coqueret, X.; Benmouna, M. *Macromol. Theory Simul.* **1998**, *7*, 599.
(19) Benmouna, F.; Coqueret, X.; Maschke, U.; Benmouna, M. *Macromolecules* **1998**, *31*, 4879.
(20) Bauer, B. J.; Briber, R. M.; Han, C. C. *Macromolecules* **1989**, *22*, 940.
(21) Briber, R. M.; Bauer, B. J. *Macromolecules* **1991**, *24*, 1899.
(22) Warner, M.; Wang, X. J. *Macromolecules* **1992**, *25*, 445.
(23) Wang, X. J.; Warner, M. *Macromol. Theory Simul.* **1997**, *6*, 27.
(24) Flory, P. J. *J. Chem. Phys.* **1942**, *10*, 51.
(25) Huggins, M. L. *J. Chem. Phys.* **1941**, *9*, 440.
(26) Dusek, K. *J. Polym. Sci. C* **1967**, *16*, 1289.
(27) Dusek, K.; Prins, W. *Adv. Polym. Sci.* **1969**, *6*, 1.
(28) Moerkerke, R.; Koningsveld, R.; Berghams, H.; Dusek, K.; Solc, K. *Macromolecules* **1995**, *28*, 1903.
(29) Maier, W.; Saupe, A. *Z. Naturforsch.* **1958**, *A13*, 564; **1959**, *A14*, 882; **1960**, *A15*, 287.
(30) Flory, P. J. *J. Chem. Phys.* **1950**, *18*, 108.
(31) James, H.; Guth, E. J. *J. Chem. Phys.* **1947**, *15*, 669.
(32) Petrovic, Z. S.; Macknight, W. J.; Koningsveld, R.; Dusek, K. *Macromolecules* **1987**, *20*, 1088.
(33) Olabisi, O.; Robeson, L. M.; Shaw, M. T. *Polymer−Polymer Miscibility*; Academic Press: New York, 1979.
(34) Technical Data Sheet for NOA65 Optical Adhesive, Norland Products, Inc., New Brunswick, NJ.
(35) Nwabunma, D.; Chiu, H.-W.; Kyu, T., unpublished results.
(36) Flory, P. J. *Macromolecules* **1979**, *25*, 101.
(37) de Gennes, P.-G. In *Polymer Liquid Crystals*; Ciferri, A., Krigbaum, W. R., Meyer, R. B., Eds.; Academic Press: New York, 1982.
(38) Amundson, K.; van Blaaderen, A.; Wiltzius, P. *Phys. Rev. E* **1997**, *55*, 1646.

MA981556Y